shown to facilitate cellular/subcellular delivery of siRNA [7–16]. Thus, a variety of ligand molecules that bind to specific receptors on cancer cells have been installed on the surface of nanoparticles [7–16]. In order to take full advantage of such targeting ligands, however, maintaining the nanoparticle structure in circulation is essential; targeting ligands can cooperatively function when distributed on the nanoparticle surface, allowing for avidity through multisite binding [13,15,17,18]. Therefore, a highly effective siRNA delivery system should result from incorporating cellular surface-targeting ability to a nanoparticle platform resistant to destabilization (or dissociation), thus maximizing the ligand binding effect.

A promising platform for systemic siRNA delivery into solid tumors is the polyion complex (PIC) micelle, constructed with block copolymers of poly(ethylene glycol) (PEG) and a polycation as an siRNA binding segment [13,16,19–22]. Charge neutralization between siRNA and the polycationic segment of the block copolymer in aqueous solution enables formation of PIC micelles, in which the siRNA-loaded PIC core is surrounded by a nonionic and hydrophilic PEG shell. This core–shell structure results in enhanced colloidal stability and reduced nonspecific interactions with charged biomacromolecules. To further increase micelle stability for *in vivo* delivery, several stabilizing approaches via hydrophobic interactions [16,23] or disulfide cross-links [13,24–26] have been investigated so far. Disulfide cross-links are noteworthy as they impart reversible stability to the micelle core upon cleavage (reduction) in the cell interior in response to the increased glutathione concentration, which is 100–1000 times higher than that in the cell exterior [27,28]. Reversible micelle stability is an important feature for nucleic acid delivery vehicles, since siRNA release into the cytoplasm is required to access the RNAi pathway.

Meanwhile, our previous studies revealed that siRNA micelles could be disrupted even with disulfide cross-linking in the core, leading to undesirable release of siRNA payloads [26]. These results suggest that the cross-linking within the micelle core may be highly localized, incapable of stabilizing the whole core structure. Thus, an additional stabilizing mechanism may further reinforce the cross-linked siRNA micelle structure, leading to longer blood circulation and enhanced tumor accumulation. Herein, cholesterol-conjugated siRNA (Chol-siRNA) [29] was utilized to stabilize micelle core structures in addition to disulfide cross-linking. Hydrophobized siRNAs are expected to suppress micelle disruption and subsequent leakage of siRNA due to hydrophobic associations of cholesterol groups [16,30]. Therefore, the combined use of a thiolated block copolymer and Chol-siRNA creates a stable, yet reversible, platform for improved systemic siRNA delivery.

In this work, we employed a functional block copolymer comprising PEG segment installed with cyclo-Arg-Gly-Asp (cRGD) peptide as the tumor-targeting hydrophilic block [13,16,31] and poly(L-lysine) (PLL) segment modified with dithiobispropionimidate (DTBP) as the cationic block [26]. DTBP modification was chosen for generating a single and stable side chain structure comprising an amidine and thiol functionality, making polyionic pairs/hydrogen bonds with siRNA phosphates in addition to disulfide cross-linking [26]. After examining the contribution of Chol-siRNA to micelle stability, the targeting ability of cRGD ligand was verified utilizing a luciferase-expressing cervical cancer (HeLa-Luc) cell line. Finally, the *in vivo* siRNA delivery efficacy of the actively-targeted/stabilized micelles was evaluated by luciferase gene silencing activity in the murine subcutaneous tumors after systemic administration, demonstrating strong potential for tumor-targeted systemic siRNA delivery.

2. Materials and methods

2.1. Materials

D_2O (99.9%), tetramethylsilane (TMS, 99.5%), boric acid, trizma base and Dulbecco's modified Eagle's medium (DMEM) were purchased from Sigma Aldrich (St. Louis, MO) and used without further purification. Dithiothreitol (DTT, molecular biology grade DNase and RNase free), ethylenediamine tetraacetic acid disodium salt dihydrate (EDTA, 99.5%) and ethidium bromide solution were supplied by Wako Pure Chemical Industries (Osaka, Japan). Dimethyl-3,3′-dithiobispropionimidate/2HCl (DTBP/HCl) and slide-a-lyzer dialysis cassettes (MWCO 3500 Da) were purchased from Thermo Scientific (Rockford, IL). Sterile HEPES (1 M, pH 7.3) was purchased from Amresco (Solon, OH). Agarose L03 TAKARA was purchased from Takara Bio Inc (Shiga, Japan) and used for gel electrophoresis. Cell Counting Kit 8 (CCK-8) was purchased from Dojindo Laboratories (Kumamoto, Japan). Cyclo-[RGDfK(C-∑-Acp)] (cRGD) peptide was synthesized by Peptide Institute Inc. (Osaka, Japan). A series of siRNAs were synthesized by Hokkaido System Science Co., Ltd. (Hokkaido, Japan) and their sequences were as follows; (1) firefly GL3 luciferase (siLuc): 5′-CUU ACG CUG AGU ACU UCG AdTdT-3′ (sense), 5′-UCG AAG UAC UCA GCG UAA GdTdT-3′ (antisense); (2) control scramble sequence (siScr): 5′-UUC UCC GAA CGU GUC ACG UdTdT-3′ (sense), 5′-ACG UGA CAC GUU CGG AGA AdTdT-3′ (antisense). Cy5 dye and Chol moiety were introduced to the 5′-end of the antisense strand and the sense strand, respectively.

2.2. Synthesis of cyclic RGD peptide-poly(ethylene glycol)-block-poly(L-lysine) (cRGD-PEG-PLL)

cRGD-PEG-PLL and methoxy-PEG-PLL (termed PEG-PLL) block copolymers (molecular weight (MW) of PEG: 12,000 Da; degree of polymerization (DP) of PLL segment: approximately 45) were synthesized as previously described [13,19,31]. The cRGD peptide was introduced to the PEG terminus of acetal-PEG-PLL through the thiazolidine ring formation between the N-terminal cysteine of cRGD and the aldehyde group generated in acetal-PEG-PLL after incubation at acidic pH [31]. The obtained polymer (yield: 112 mg, 86%) was characterized at 22 °C by ^{1}H NMR (JEOL ECS-400, JEOL, Tokyo, Japan). The amount of cRGD conjugated to the polymer was estimated from ^{1}H NMR spectrum based on the peak intensity ratio of phenyl protons in cRGD peptide (D-Phe, δ = 7.2–7.4 ppm) to ethylene protons in PEG ($-CH_2CH_2-$, δ = 3.6–3.8 ppm) (Fig. S1). The cRGD introduction rate was calculated to be approximately 70%.

2.3. Synthesis of cyclic RGD peptide-poly(ethylene glycol)-block-poly(L-lysine modified with 1-(3-mercaptopropyl)amidine) (cRGD-PEG-PLL(MPA))

cRGD-PEG-PLL(MPA) was synthesized by introducing MPA moieties into the lysine primary amines in cRGD-PEG-PLL using DTBP, as shown in Scheme 1 [26]. Briefly, cRGD-PEG-PLL (50 mg, 0.1 mmol amines) was dissolved in 100 mM borate buffer (pH 9.0) (10 mL), followed by the addition of DTBP/HCl (69 mg, 0.2 mmol). The reaction solution was stirred at 25 °C for 45 min and then dialyzed (MWCO 3500 Da) against 10 mM PBS (pH 6.0) for 2 h and distilled water for 2 h. The dialyzed solution was lyophilized after filtration (yield: 53.9 mg, 80%). The substitution degree of MPA groups in the obtained polymer was determined from the ^{1}H NMR spectrum based on the peak intensity ratio of β, γ and δ methylene protons in PLL side chains ($-(CH_2)_3-$, δ = 1.3–1.9 ppm) to mercaptoethyl protons in MPA moieties ($HS-(CH_2)_2-$, δ = 2.7–2.9 ppm) (Fig. 1), demonstrating quantitative introduction (>97%). In a similar manner, PEG-PLL(MPA) without cRGD peptide was synthesized by the reaction of PEG-PLL with DTBP (Scheme 1). For PEG-PLL(MPA), PEG-PLL (300 mg, 0.71 mmol amines) and DTBP/HCl (439 mg, 1.4 mol) were used (yield: 299 mg, 73%). Quantitative introduction of MPA group (>99%) was also confirmed by ^{1}H NMR analysis (Fig. S2).

2.4. Polyionic complexation of block copolymers with siRNA

cRGD-PEG-PLL(MPA) (or PEG-PLL(MPA)) block copolymer was dissolved in 10 mM HEPES buffer (pH 7.4) and incubated with 100 mM DTT at 25 °C for 15 min for disulfide reduction. The reduced polymer solution was mixed with siRNA dissolved in the same buffer (15 μM siRNA) at different molar charge ratios of the block copolymer to siRNA, i.e., amidines and primary amines in the block copolymer/phosphates in siRNA. To proceed disulfide cross-linking in the PIC core, PIC solutions (10 μM siRNA) were dialyzed (MWCO 3500 Da) against 5 mM HEPES (pH 7.4) containing 0.5% (v/v) DMSO for 2 days and 5 mM HEPES (pH 7.4) for 2 days. Dialyzed PIC solutions were filtered (0.22 μm) before characterization. In a similar manner, control PICs without Chol moieties were also prepared with PEG-PLL(MPA) and siRNA. For *in vivo* experiments, micelle solutions were dispersed in 5 mM HEPES (pH 7.4) and made isotonic by addition of 1.5 M NaCl to a final concentration of 150 mM.

2.5. Static and dynamic light scattering (SLS and DLS) analyses

SLS and DLS measurements were performed with a ZetaSizer Nano ZS instrument (Malvern Instruments Ltd., Worcestershire, UK) equipped with a He–Ne laser (λ = 633 nm) as the incident beam. All measurements were made at 25 °C and a detection angle of 173°. PIC samples (10 μM siRNA, 18 μL) dispersed in 5 mM HEPES buffer (pH 7.4) were loaded into a low-volume cuvette (Zen 2112) for each analysis.

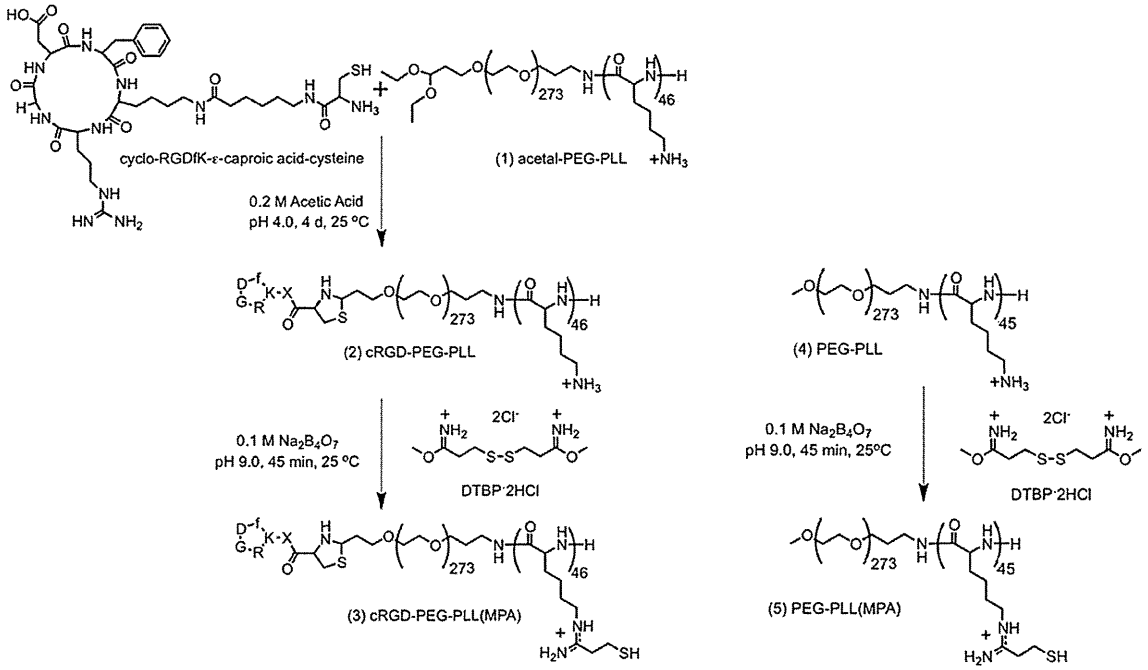

Scheme 1. Synthesis schemes of cRGD-PEG-PLL(MPA) and PEG-PLL(MPA).

Scattered light intensity (SLI) was measured to monitor micelle formation, using a constant attenuator setting in the instrument. Cumulant size, polydispersity index (PDI), and size distribution (intensity-weighted) histogram were calculated based on the autocorrelation function of samples, with automated attenuator adjustment and multiple scans (typically 12–30 scans) for optimal accuracy.

2.6. Fluorescence correlation spectroscopy (FCS) measurement

Diffusion time of fluorescently-labeled micelles (or naked siRNA) was measured by FCS using samples prepared with Cy5-labeled siRNA (Cy5-siRNA). Samples containing 10 μM Cy5-siRNA were diluted with PBS containing 10% FBS, followed by 1 h incubation. Then, the samples were placed into an 8-well Lab-Tek chambered borosilicate cover-glass (Nalge Nunc International, Rochester, NY) and measured with a combination system of ConfoCor3 module and LSM510 equipped C-Apochromat 40×, N.A. 1.2 water immersion objective (Carl Zeiss, Oberkochen, Germany) (sampling time: 10 s, repeating time: 10). A He–Ne laser (633 nm) was used for excitation of Cy5-siRNA and emission was filtered through the corresponding band-pass filter. The measured autocorrelation curves were fitted with the Zeiss Confocor3 software package to obtain the corresponding diffusion time. The obtained diffusion time was converted to the corresponding hydrodynamic diameter by the Stokes-Einstein equation.

2.7. Gel electrophoresis

Agarose gel was prepared by adding agarose (0.7 g) to a TBE buffer (70 mL) prepared with trizma base (10.8 g), boric acid (5.5 g) and EDTA/2Na (74 mg) in pure water (1 L). The mixture was heated to dissolve the agarose powder and then allowed to cool down before adding ethidium bromide (1 μL). Micelle solutions (2 μL) with or without DTT (200 mM DTT) were mixed with dextran sulfate solutions (2 μL). The concentrations of dextran sulfate groups were set at 0, 1.0, 1.5, 2.0 and 3.0 times equivalent to the siRNA phosphates. After incubation for 2 h at 25 °C, each sample was loaded on the gel and electrophoresed (100 V, 30 min) in TBE running buffer. After electrophoresis, gel images were captured by a Typhoon 9410 instrument equipped with a 532 nm laser. Also, micelle samples were subjected to the electrophoresis (50 V, 30 min) after incubation with different amounts of anionic lipid, DOPS (1,2-dioleoyl-sn-glycero-3-phospho-L-serine sodium salt), for 8 h at 25 °C.

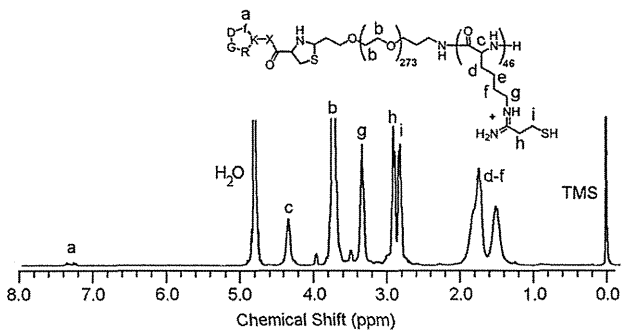

Fig. 1. ^{1}H NMR spectrum of cRGD-PEG-PLL(MPA), recorded in D_2O (10 mg/mL) at 25 °C.

2.8. Cellular uptake

Luciferase-expressing human cervical cancer cells, HeLa-Luc (Caliper Life-Science, Hopkinton, MA), were seeded into 6-well plates (100,000 cells/well) and incubated in DMEM containing 10% fetal bovine serum (FBS) (Dainippon Sumitomo Pharma Co. Osaka, Japan) (1.5 mL) for 24 h. The culture media were then exchanged with fresh media containing micelle samples prepared with Cy5-siRNA (siRNA concentration: 333 nM). Cells were incubated in the presence of micelles for 75 min at 37 °C and then further incubated in the absence of micelles for 8 h after medium exchange. The cells were harvested by trypsinization, followed by flow cytometric analyses using a BD LSR II instrument (BD Biosciences, San Jose, CA) and BD FACS Diva software (BD Biosciences).

2.9. In vitro luciferase assay

HeLa-Luc cells were seeded in 35 mm dishes (25,000 cells/dish) and incubated in DMEM containing 10% FBS (2 mL) for 24 h. Then, the culture media were exchanged with fresh media (2 mL) containing 100 μM luciferin (Summit Pharmaceutical International, Tokyo, Japan) and micelle samples (200 nM siRNA). For each analysis, control samples were prepared by treating cells with 5 mM HEPES buffer (pH 7.4). Samples were placed into a Kronos real-time photon countable incubator (ATTO Corp., Tokyo, Japan) at 37 °C and 5% CO_2 and the luminescence intensity (counts) was measured periodically over 50 h. Relative luminescence intensity was determined by normalizing the average luminescence intensity of treated samples ($n = 4$) to the average luminescence intensity of control samples ($n = 4$).

2.10. Cytotoxicity assay

HeLa-Luc cells were seeded in 24-well plates (20,000 cells/well) and incubated in DMEM containing 10% FBS (0.5 mL) for 24 h. Thereafter, the culture media were replaced with fresh media containing micelle samples at varying siRNA concentrations and cells were further incubated for 48 h. Then, CCK-8 solution (1 μL/10 μL medium) was added and samples were further incubated at 37 °C for 1 h. Cell viability was determined from the absorbance of extracellular media at 450 nm,

which was measured using a BIO-RAD 680 microplate reader (Bio-Rad, CA). All data are expressed relative to untreated control cells ($n = 6$).

2.11. Blood circulation behavior

All animal experimental procedures were performed in accordance with the policies of the Animal Ethics Committee of The University of Tokyo. The blood circulation property of siRNA-loaded micelles was determined by IVRT-CLSM observation of live mice (BALB/c nude, female, 8 weeks old) (Charles River laboratories, Tokyo, Japan) using a Nikon A1R CLSM system attached to an upright ECLIPSE FN1 (Nikon Corp., Tokyo, Japan) equipped with a 20×, 640 nm diode laser, and a band-pass emission filter of 700/75 nm, as previously described [32]. The mice were anesthetized with 2–3% isoflurane (Abbott Japan Co., Ltd., Tokyo, Japan) using a Univenter 400 anesthesia unit (Univentor Ltd., Zejtun, Malta) and placed onto the temperature-controlled microscope stage. Blood vessels in the ear-lobe dermis were observed after tail vein injection of micelles prepared with Cy5-siRNA (3.6 nmol Cy5-siRNA/mouse, $n = 3$), as they were clearly observed without surgery (thus non-invasive) and were unaffected by the cardiac beat (thus steadily observed). The obtained images were analyzed by selecting regions of interest (ROIs) within blood vessels for determining the average fluorescence intensity at each time point. To produce blood circulation profiles shown in Fig. 5A, the vein fluorescence intensities were expressed as a relative value to the highest (1.0) and the lowest (0) obtained through the observation. In addition, the time point for the highest fluorescence intensity was defined as $t = 0$.

2.12. Tumor accumulation

HeLa-Luc cells (2.6×10^6 cells) were injected under the skin of mice for preparation of donor tumors. After 2 weeks, the donor tumors were excised and cut into pieces, then transplanted under the skin of host mice. After 8 days, the subcutaneous tumor-bearing mice were subjected to tail vein injection of micelles prepared with Cy5-siRNA (1.8 nmol Cy5-siRNA/mouse, $n = 4–5$). After 4 h, they were sacrificed, and tumors (and major organs) were excised, followed by fluorescence quantification using an IVIS instrument equipped with Living Image software. Total photon counts were normalized to the illumination time and the sample area as follows: fluorescence intensity = total photons/[illumination time (s) × area (cm^2)]. Further normalization was performed by dividing the fluorescence intensity from the tumors treated with RGD-free controls.

2.13. In vivo luciferase assay

Subcutaneous HeLa-Luc tumor models were prepared by *in vivo* passage of tumor fragments, as described in the former section. After 8 days, the tumor-bearing mice were subjected to the tail vein injection of micelle samples (1.8 nmol siRNA/mouse/injection, $n = 5$) at 48 h, 38 h and 24 h before measurement. A luciferin solution (50 mM, 200 μL) was injected intraperitoneally 25 min prior to measurement to obtain the stable luminescence intensity from tumors. The luminescence intensity (counts) was recorded using an IVIS instrument under the same condition for each image (acquisition time: 5 s, binning: small, f/stop: 1, and field of view: D). Tumor volumes were determined by manual measurement with a caliper and calculated using the following equation: volume = $ab^2/2$, where a is the long axis and b is the short axis measured. The luminescence intensity obtained from sample-treated tumors was normalized to the tumor volume and further to that from buffer-treated control tumors: relative luminescence intensity = total photons of sample/sample-treated tumor volume (cm^3)/total photons of buffer control/control-treated tumor volume (cm^3).

2.14. Data analysis

The experimental data were analyzed by Student's t-test. $p < 0.05$ was considered statistically significant.

3. Results and discussion

3.1. Synthesis of block copolymers and their characterizations

In order to create actively-targeted and stabilized PIC micelles, a functional block copolymer was synthesized to comprise a targeting ligand, cationic charges, and free thiol groups (Scheme 1). The cRGD peptide was utilized as the ligand for tumor targeting through specific binding to $\alpha_v\beta_3$ and $\alpha_v\beta_5$ integrins, which are overexpressed on various cancer cells [33,34]. Also, DTBP was selected as the thiolation reagent because a cationic amidine group is concurrently introduced following reaction with lysine amines, preserving the polymer ability to form ion pairs with siRNA phosphates [26]. First, the cRGD peptide was conjugated to acetal-PEG-PLL by thiazolidine ring formation between the aldehyde generated on the PEG terminus at low pH and the N-terminal cysteine residue contained on the cRGD peptide [31]. Next, cRGD-PEG-PLL (or PEG-PLL as a non-targeted control) was reacted with DTBP under basic conditions to generate cRGD-PEG-PLL(MPA) (or PEG-PLL(MPA)) bearing the desired amidine and thiol functionalities in PLL side chains. Successful introduction of cRGD (71%) and MPA modification of amines (97%) was confirmed by ^{1}H NMR analysis of the cRGD-PEG-PLL(MPA) reaction product (Fig. 1). Similarly, quantitative reaction of DTBP with lysine amines in PEG-PLL lacking cRGD (>99%) was also confirmed (Fig. S2).

3.2. Preparation and characterization of Chol-siRNA micelles

Micelle formation behavior with Chol-siRNA was investigated in terms of SLI, size and PDI by light scattering measurements (SLS and DLS). SLI values were utilized for confirming whether i) the signal intensity (or S/N ratio) of samples was suitable for fitting and ii) the polymer/siRNA mixtures formed multimolecular assemblies (i.e. micelles) prior to fitting. The size and the PDI were then determined by appropriate fitting. PEG-PLL(MPA) was mixed with Chol-siRNA or Chol-free siRNA as a control at varying residual molar charge ratios of the block copolymer to siRNA (+:− ratio). SLI values observed for polymer/Chol-siRNA mixture increased sharply in +:− ratios from 0 to 1.2 (Fig. 2A), similar to those for Chol-free siRNA mixture, indicating formation of PIC micelles due to the charge-neutralization between the polymer and siRNA. At

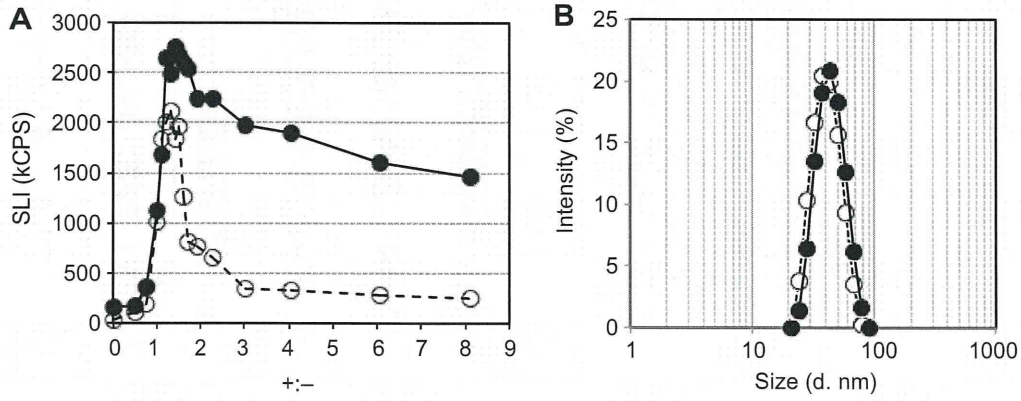

Fig. 2. Light scattering behavior of PEG-PLL(MPA) polymer and siRNA mixtures in 10 mM HEPES buffer (pH 7.4) at 25 °C. Open circles: Chol-free siRNA, closed circles: Chol-siRNA. A) SLI of mixtures at different +:− ratios. B) Intensity-weighted histograms of mixtures at +:− = 1.4.

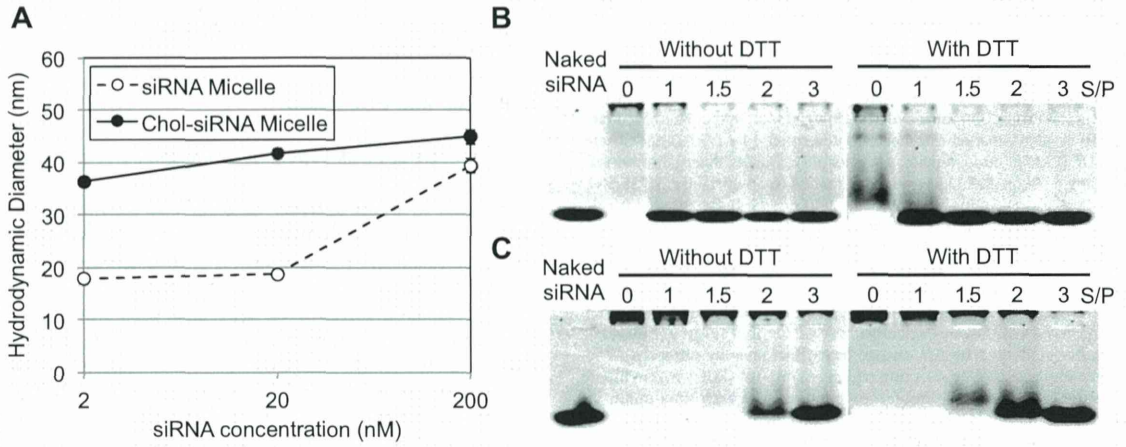

Fig. 3. Micelle stability assays. A) Change in size of Chol-free/Cy5-siRNA micelles and Chol/Cy5-siRNA micelles associated with dilution in 10% FBS-containing PBS. The diffusion time was measured by FCS and then the hydrodynamic diameter was calculated from the diffusion time (or diffusion coefficient) by the Stokes-Einstein equation. Each micelle was incubated for 1 h before measurements. Data represent the average value ± standard deviation (sampling time = 10 s, repetition time = 10). B and C) Agarose gel electrophoresis of siRNA micelles prepared with B) Chol-free siRNA and C) Chol-siRNA (0.3 μg) incubated with different concentrations of dextran sulfate under 0 or 100 mM DTT for 2 h. S/P ratio was defined as the molar ratio of sulfate groups in dextran sulfate to phosphate groups in siRNA.

+:− = 1.4, Chol-siRNA micelles were 43 ± 2 nm ($n = 3$) in cumulant diameter, and exhibited the lowest level of PDI (Fig. S3) as well as the highest SLI in the charge ratios tested. This slightly shifted +:− ratio from the charge-stoichiometric point is presumably due to the fact that complete ion-pair formation within PICs can be sterically hindered in block copolymers [26,35]. The intensity-weighted histograms at this mixing ratio clearly show the similar size distributions between Chol-siRNA and Chol-free micelles (Fig. 2B). These results confirm that the Chol moiety did not alter the micelle formation behavior between PEG-PLL(MPA) and siRNA at +:− <1.4. Note that a remarkable difference was observed between the two micelle formulations in their SLI values at +:− >1.4. The Chol-free siRNA mixture showed a drastic decrease in SLI, possibly due to the binding of a charge-excess amount of block copolymers to siRNA, generating electrostatic repulsion between PICs, and thus impeding their self-assemble into micelle structures [26]. In contrast, the Chol-siRNA mixture greatly resisted such decrease in SLI, indicating a stronger association force of Chol-siRNA PICs that can overcome electrostatic repulsion [30]. Meanwhile, the effect of MPA moieties in PEG-PLL(MPA) was additionally examined on the polyion complexation with Chol-siRNA by comparing with non-thiolated PEG-PLL. The PEG-PLL/Chol-siRNA mixtures showed the PDI of >0.18 in the tested mixing ratios from 0 to 4 (Fig. S3). These results demonstrate the crucial role of MPA moieties for the uniform micelle formation between Chol-siRNA and PEG-PLL(MPA); a possible explanation for the role of MPA moiety is that a higher degree of MPA moiety, i.e., thiol and guanidino groups, in the polycationic side chain could allow stronger intermolecular interactions with each other and/or siRNA through hydrogen bonding, dipole–dipole interactions, or Van der Waals force,

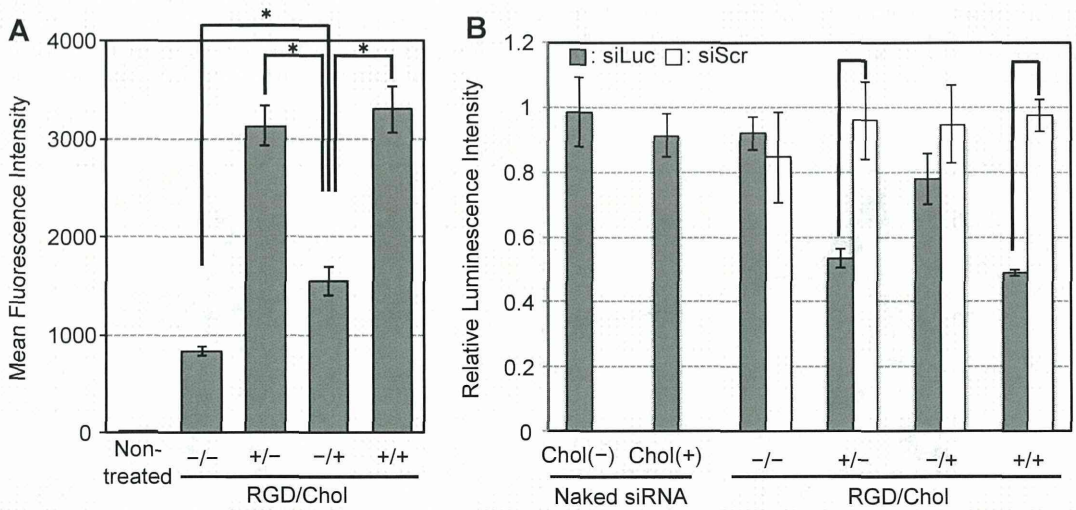

Fig. 4. A) Cellular uptake of Cy5-siRNA micelles in cultured HeLa-Luc cells, evaluated by flow cytometry. Cells were incubated with micelles for 75 min before medium change, and then further incubated for 8 h at 37 °C. Data represent the average value ± standard deviation ($n = 4$, *: $p < 0.05$). B) Gene silencing activity of naked siRNAs and siRNA micelles at 200 nM siRNA in cultured HeLa-Luc cells. Luminescence intensity was measured after 50 h incubation with siRNA samples and normalized to the value of nontreated control cells. Data represent the average value ± standard deviation ($n = 4$, *: $p < 0.05$).

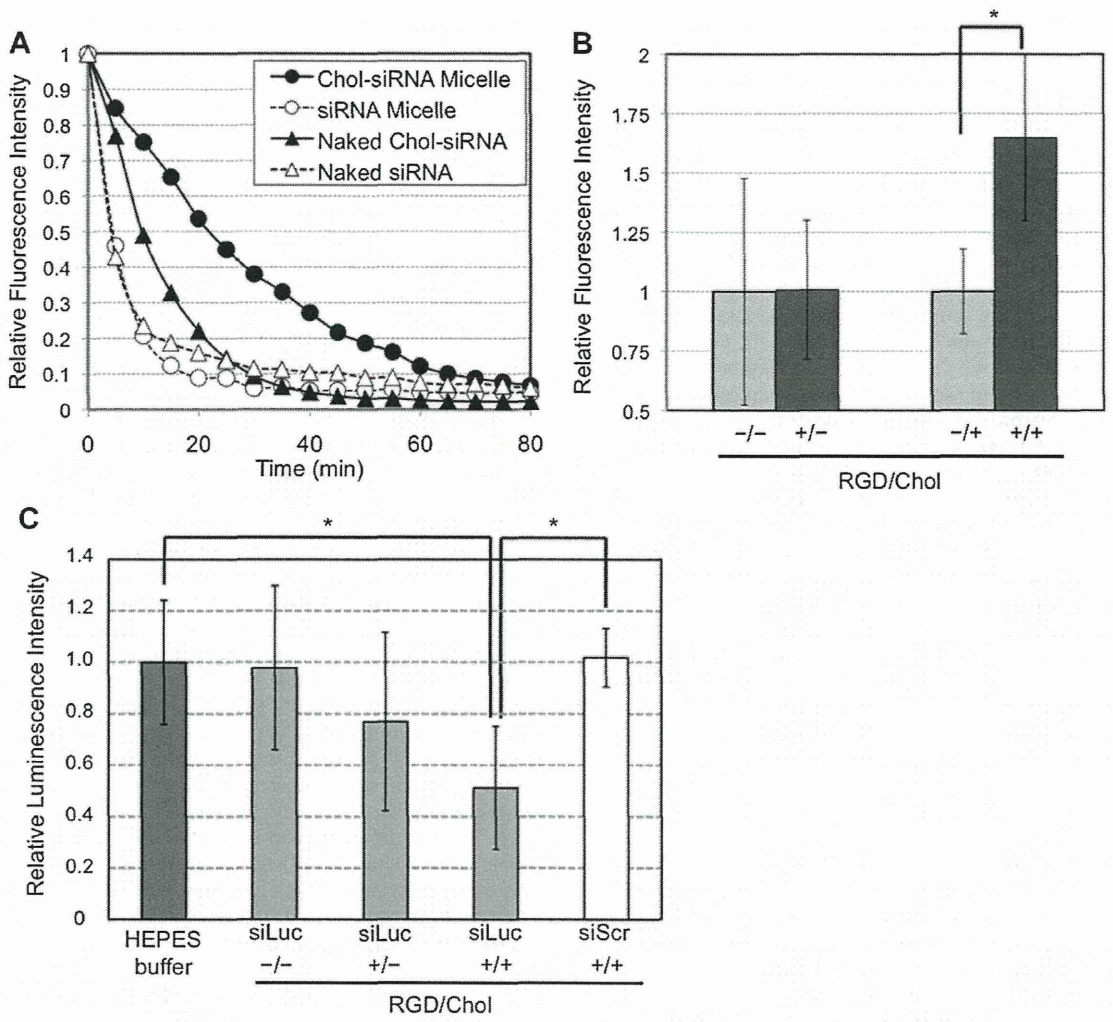

Fig. 5. *In vivo* performance of siRNA micelles. A) Blood circulation profiles, determined by IVRT-CLSM after intravenous injection (3.6 nmol siRNA/mouse) into BALB/c nude mice (open triangle: naked Chol-free/Cy5-siRNA, closed triangle: naked Chol/Cy5-siRNA, open circle: Chol-free/Cy5-siRNA micelles and closed circle: Chol/Cy5-siRNA micelles). Data represent the average value ($n = 3$). B) Relative accumulation of actively-targeted siRNA micelles to non-targeted controls in subcutaneous HeLa-Luc tumors (1.8 nmol siRNA/mouse) 4 h after intravenous injection into BALB/c nude mice. Fluorescence intensity from excised tumors was measured with an IVIS instrument, followed by the normalization as described in the Section 2.12. Data represent the average value ± standard deviation ($n = 4$ or 5, *: $p < 0.05$). C) Luciferase gene silencing activity of siRNA micelles in subcutaneous HeLa-Luc tumors. siRNA micelles were intravenously injected (1.8 nmol siRNA/mouse/injection) at 48, 38 and 24 h prior to measurement of the luminescence intensity from the excised tumors. The obtained luminescence intensity was normalized to that from the buffer-treated control tumors and the tumor volume. Data represent the average value ± standard deviation ($n = 5$, *: $p < 0.05$).

directed toward more uniform and stable micelle formation. Altogether, siRNA micelles prepared at +:− = 1.4 were used for subsequent experiments owing to the similarity in size between the two formulations as well as the sample homogeneity (lowest PDI). It should be further noted that the size distribution histograms were similar between non-targeted Chol-siRNA micelles prepared with PEG-PLL(MPA) and targeted Chol-siRNA micelles prepared with cRGD-PEG-PLL(MPA) at +:− = 1.4 (Fig. S4), suggesting that the cRGD peptide does not affect PIC formation with Chol-siRNA.

3.3. Stability of Chol-siRNA micelles

To confirm the stabilizing effect of cholesterol, the sizes of Chol-siRNA micelles and Chol-free micelles were determined under diluted conditions in 10% FBS-containing PBS by FCS measurement, which allows monitoring of the hydrodynamic size (or diffusion coefficient) of fluorescently labeled nanoparticles even in the presence of abundant serum proteins [16]. Indeed, this measurement determined the diffusion coefficients of Cy5-siRNA or Chol/Cy5-siRNA molecules complexed with the polymers, followed by conversion to hydrodynamic diameters based on the Stokes-Einstein equation (Fig. 3A). Whereas the original size of Chol-free micelles (ca. 40 nm) was maintained at 200 nM Cy5-siRNA, further dilution below 20 nM Cy5-siRNA dramatically decreased the micelle size, indicating disruption of Chol-free micelles upon dilution in the presence of FBS. It should be noted that the size of disrupted micelles (ca. 20 nm) was significantly larger than that of naked Cy5-siRNA (ca. 5 nm), suggesting that the micelles might be fragmented into small PIC fractions with a low association number of Cy5-siRNAs and block copolymers upon dilution, possibly due to limited intermolecular disulfide cross-linking within the micelle core. In contrast, Chol-siRNA micelles maintained their original size after dilution with 10% FBS, demonstrating the stabilizing effect of Chol moieties for maintaining micelle structure integrity.

Next, to further investigate micelle destabilization due to disulfide reduction as well as the stabilizing effect of Chol moieties, agarose gel electrophoresis of micelle samples was performed after incubation with or without DTT in the presence of varying concentrations of dextran sulfate (MW = 5000). This strong polyanion was used for mimicking the negatively charged extracellular matrixes, as a recent study reported that those polyanionic components play a crucial role for the destabilization of blood circulating siRNA PICs [36]. The stabilizing effect of Chol moiety was again observed upon analysis of siRNA release induced by the counter polyanions. Chol-siRNA micelles required larger amounts of dextran sulfate for the appearance of the released siRNA band, compared to Chol-free micelles (Fig. 3B and C). Futhermore, the decreased stability under the reductive conditions was confirmed for Chol-siRNA micelles, as the incubation under 100 mM DTT apparently decreased the amount of dextran sulfate required to release free siRNA from micelles (Fig. 3B and C). The similar facilitated siRNA release profiles were also observed for Chol-siRNA micelles under a cytoplasm-mimicking condition (10 mM DTT and 150 mM NaCl) in comparison with a cell exterior-mimicking condition (10 μM DTT and 150 mM NaCl) (Fig. S5A and B). Nevertheless, the modest difference between non-reductive and reductive conditions implies the significant, yet restricted contribution of disulfide cross-linking to the resistance of micelles against a strong polyanion. Note that the stabilizing effect of disulfide cross-linking was more evident under milder conditions where micelle samples were incubated with an anionic lipid molecule (DOPS). In this experiment, micelle sensitivity to reductive conditions was clearly observed even for Chol-free micelles (Fig. S5C and D).

3.4. *In vitro efficacy of actively-targeted/stabilized micelles*

To verify the biological effect of cRGD ligand as well as the stabilizing effect of Chol-siRNA, cellular uptake efficiencies of siRNA micelle formulations were compared by flow cytometric analyses. In this experiment, the fluorescence intensity of HeLa-Luc cells was determined after their treatment with micelles prepared with Cy5-siRNA. Note that HeLa-Luc cells were chosen as a target cell line because they overexpress integrins, especially $\alpha_v\beta_5$, on their cellular surface (Fig. S6) [31,37], and are thus appropriate for assessing the cRGD effect on cellular uptake of siRNA. Significantly higher fluorescence intensity was observed for cRGD-installed micelles, i.e., RGD(+)/Chol(−) and RGD(+)/Chol(+) micelles, in comparison with control micelles without cRGD, i.e., RGD(−)/Chol(−) and RGD(−)/Chol(+) micelles (Fig. 4A). These results highlight the effect of cRGD on the enhanced cellular uptake of siRNA micelles. In the absence of cRGD ligand, the cells incubated with RGD(−)/Chol(+) micelles showed modestly higher fluorescence intensity than those incubated with RGD(−)/Chol(−) micelles, indicating that Chol-siRNA facilitated the cellular uptake of RGD(−) micelles. Apparently, the Chol-siRNA was more effective for improving the cellular uptake of non-targeted RGD(−) micelles, compared to the targeted RGD(+) micelles. These different effects of Chol-siRNA can be explained from the standpoint of cellular uptake rate of micelles; the targeted RGD(+) micelles may be internalized more rapidly and less affected by micelle stability in cell culture conditions, compared to the non-targeted RGD(−) micelles.

Next, *in vitro* gene silencing ability of the actively-targeted/stabilized (RGD(+)/Chol(+)) micelles was evaluated by comparing with those of the other micelle formulations. siRNA for luciferase gene, i.e., siLuc, was selected for this luminescence-based gene silencing assay, which allows quantitative determination of gene silencing by comparing the luminescence intensity among samples. Fig. 4B shows the relative luminescence intensity of cells treated with each siRNA micelle (or naked siRNA) at 200 nM siRNA after 50 h incubation. The observed *in vitro* gene silencing activity is in good agreement with the results from the cellular uptake study (Fig. 4A); as cRGD-installed, RGD(+)/Chol(+) and RGD(+)/Chol(−) micelles achieved the most efficient luciferase gene silencing, followed by the RGD(−)/Chol(+) micelles and the RGD(−)/Chol(−) micelles. Actively-targeted micelles prepared with siScr induced no significant decrease in relative luminescence intensity, confirming the sequence-specific gene silencing activity of actively-targeted micelles. Consequently, the cRGD ligands installed on the micelle surface enhanced *in vitro* gene silencing activity of siRNA micelles regardless of the Chol moiety conjugated to siRNA. This is consistent with the result seen in Fig. 3A; the Chol-free micelles could avoid the rapid dissociation in the 10% serum-containing PBS under 200 nM siRNA corresponding to the transfection condition, presumably enabling ligand-mediated rapid cellular uptake. It should be noted in this regard that the Chol-free siRNA micelles prepared with cRGD-PEG-PLL without thiol (or other stabilizing) moieties induced no gene silencing under similar conditions as we reported previously [13], indicating the impact of disulfide cross-linking on gene silencing efficiency.

Cell viability following treatment with siRNA micelles was also examined in order to exclude the possibility of cytotoxic effects on the gene silencing activity of siRNA micelles. RGD(+)/Chol(−) micelles and RGD(+)/Chol(+) micelles, which showed the highest gene silencing activity, were subjected to a cell viability assay using the commercially available CCK-8 kit, based on a water soluble tetrazolium salt (WST-8). Neither micelle formulation induced significant cytotoxicity even at a high concentration of siRNA (1000 nM) (Fig. S7), indicating negligible cytotoxic effects of siRNA micelles at concentrations used for the gene silencing studies. Considering that homopolymer PLLs with a high molecular weight (e.g. 27 kDa) are known to induce significant cytotoxicity due to their cationic charges [38], this negligible cytotoxicity of the siRNA micelles might be the result that they were composed of a relatively shorter PLL segment and equipped with a PEG outer layer that masked the charged component.

3.5. *In vivo efficacy of actively-targeted/stabilized micelles*

Since enhanced micelle stability and active targeting ability were both demonstrated under *in vitro* conditions (Figs. 3 and 4A and B), the *in vivo* behaviors of actively-targeted/stabilized micelles were investigated following systemic administration. The longevity of siRNA micelles in the bloodstream is a critical factor for tumor accumulation of macromolecules. Prolonged circulation results in increased contact opportunity for actively-targeted micelles with the cellular surface receptors in tumor tissues.

First, the blood circulation property of fluorescently-labeled micelles (prepared with Cy5-siRNA) was evaluated by IVRT-CLSM, which can continuously monitor the fluorescence intensity of Cy5-siRNA (or its micelles) circulating in the blood of mice immediately after intravenous injection (Fig. S8A). Fluorescence intensities determined from ROIs selected within the vein were plotted against time to compare blood retention profiles of different micelle formulations (Fig. 5A). In this regard, non-targeted micelles were utilized for simply validating the effect of Chol-siRNA encapsulated within the micelles on blood retention. Chol-free micelles were rapidly eliminated from circulation, similar to naked siRNA, and consequently their blood half-life ($T_{1/2}$) was within 5 min. In sharp contrast, Chol-siRNA micelles showed significantly longer blood retention time ($T_{1/2} = >20$ min, $p < 0.05$) than Chol-free micelles. This prolonged blood circulation observed for Chol-siRNA micelles is in good agreement with the results demonstrating higher stability against dilution with serum-containing PBS (Fig. 3A) and improved resistance to polyanion

exchange with polysulfates (Fig. 3C). It is also worth mentioning that the elimination of Chol-siRNA micelles from the bloodstream followed a single exponential decay (or a one-compartment model in pharmacokinetics) (Fig. S8B), suggesting that the Chol-siRNA micelles were eliminated mainly from the kidney without being distributed into peripheral tissues. This is supported by the result that the Chol-siRNA micelles (or the siRNA payloads) were mainly accumulated in the kidney after systemic administration (Fig. S9). Note that the blood retention time of naked Chol-siRNA was modestly longer than those of naked Chol-free siRNA. This may be due to interaction of Chol-siRNA with lipoproteins in the bloodstream leading to compromised renal filtration [39].

Next, the tumor-targeting ability of cRGD-installed micelles was investigated by measuring their accumulation in subcutaneous HeLa-Luc tumors. Fluorescently-labeled micelles were administered by tail vein injection and tumors were excised after 4 h followed by measurement of the fluorescence intensity of each tumor mass with an IVIS instrument. While there was almost no difference in fluorescence intensity between Chol-free micelles with and without cRGD, significantly higher fluorescence intensity was observed for Chol-siRNA micelles equipped with cRGD, compared to those without cRGD (Fig. 5B). These results indicate that the cRGD ligand enabled more efficient tumor accumulation of the highly stabilized Chol-siRNA micelles following systemic administration, presumably due to the enhanced avidity of cRGD ligands to $\alpha_v\beta_3/\alpha_v\beta_5$ integrin receptors on cancerous cells and also tumor-associated endothelial cells [13,33,34]. Intratumoral distribution of RGD(+)/Chol(+) micelles was further examined by continuous CLSM observation of the subcutaneous tumor tissue after systemic administration. The CLSM image captured at 80 min after injection displays massive distribution of the micelles in the tumor tissue through the blood vessels (Fig. S10). Importantly, there were no significant differences in healthy organ/tissue accumulation between non-targeted and actively-targeted micelles ($p > 0.05$) (Fig. S9), demonstrating tumor-selective targeting of RGD(+)/Chol(+) micelles.

Finally, the *in vivo* gene silencing activity of siRNA micelles was investigated through luciferase gene silencing (luminescence measurement) in subcutaneous HeLa-Luc tumors, similar to the luminescence-based assay used for *in vitro* experiments. At 48 h after the initial injection of samples (total 3 intravenous injections), luciferin solution was intraperitoneally injected into mice, followed by measurement of the luminescence intensity in the tumor tissues with an IVIS instrument (Fig. 5C and Fig. S11). Non-targeted RGD(−)/Chol(−) micelles did not decrease tumor luminescence intensity, whereas the actively-targeted, RGD(+)/Chol(−) and RGD(+)/Chol(+) micelles did reduce tumor luminescence intensities compared to buffer-treated controls. In particular, the actively-targeted/stabilized, RGD(+)/Chol(+) micelles achieved significant decrease in the luminescence intensity ($p < 0.05$ for buffer-treated controls). It should be noted that the RGD(+)/Chol(+) micelles carrying siScr as a control sequence caused no decrease in the luminescence intensity, demonstrating sequence-specific gene silencing (i.e. RNAi) activity of the actively-targeted/stabilized micelles. In addition, it was also confirmed that all the tested micelles did not induce significant changes in the body weight of tumor-bearing mice (Table S1). In total, actively-targeted and stabilized micelles were more effective in delivering intact (thus active) siRNA to the cytoplasm of tumor cells following systemic administration. The present study particularly focused on the separate functionalization of the macromolecular components, i.e., PEG-PLL and siRNA, for construction of the multifunctional formulation, i.e., actively-targeted/stabilized micelles. This approach permitted the facile functionalization based on a simple chemistry, which is in contrast to the previously developed block copolymer modified with 2-iminothiolane, where two functional groups, open chain and closed ring structures, are equilibrated in the side chain of PLL [13].

4. Conclusions

Actively-targeted and stabilized PIC micelles were constructed with Chol-siRNA and PEG-PLL comprising the cRGD ligand at the PEG terminus and thiol (and amidine) functionality in PLL side chains, for systemic siRNA delivery to solid tumors. The Chol modification of siRNA allowed the production of PIC micelles at wider mixing ratios above the charge-stoichiometric point and dramatically stabilized the micelle structure, resulting in the enhanced blood circulation property of siRNA micelles. Further, the active targeting ability of the cRGD ligand was proven by enhanced cellular uptake *in vitro* and also enhanced tumor accumulation *in vivo* following systemic administration. Ultimately, the synergistic effect of active targetability and improved stability enabled significant sequence-specific gene silencing in the subcutaneous tumor tissue following systemic administration of siRNA micelles. The results obtained in this study highlight the importance of additional stabilizing mechanisms in PIC micelle systems, and that stabilization can be achieved from both the polymer component and the siRNA component used. Here, Chol-conjugation to siRNA reinforced the limited effect of disulfide cross-linking, thus improving the active targetability of nanoparticulate formulations for systemic transport of siRNA into tumor tissues.

Acknowledgments

This research was financially supported by the Funding Program for World-Leading Innovate R&D in Science and Technology (FIRST) (JSPS), Grants-in-Aid for Scientific Research of MEXT (JSPS KAKENHI Grant Numbers 25000006 and 25282141), the Center of Innovation (COI) Program (JST), Grants-in-Aid for Scientific Research of MHLW, National Institute of Biomedical Innovation and Mochida Memorial Foundation for Medical and Pharmaceutical Research.

Appendix A. Supplementary data

Supplementary data related to this article can be found online at http://dx.doi.org/10.1016/j.biomaterials.2014.05.041.

References

[1] Fire A, Xu S, Montogomery M, Kostas S, Driver S, Mello C. Potent and specific genetic interference by double stranded RNA in caenorhabditis elegans. Nature 1998;391:806–11.
[2] Elbashir SM, Harborth J, Lendeckel W, Yalcin A, Weber K, Tuschl T. Duplexes of 21-nucleotide RNAs mediate RNA interference in cultured mammalian cells. Nature 2001;411:494–8.
[3] Burnett JC, Rossi JJ. RNA-based therapeutics: current progress and future prospects. Chem Biol Rev 2012;19:60–71.
[4] Carthew R, Sontheimer E. Origins and mechanisms of miRNA and siRNAs. Cell 2009;136:642–55.
[5] Turner J, Jones S, Moschos S, Lindsay M, Gait M. MALDI-TOF mass spectral analysis of siRNA degradation in serum confirms an RNase A-like activity. Mol Biosyst 2007;3:43–50.
[6] Van de Water F, Boerman O, Wouterse A, Peters J, Russel F, Masereeuw R. Intravenously administered short interfering RNA accumulates in the kidney and selectively suppresses gene function in renal proximal tubules. Drug Metab Dispos 2006;34:1393–7.
[7] Schiffelers RM, Ansari A, Xu J, Zhou Q, Tang Q, Strom G, et al. Cancer siRNA therapy by tumor selective delivery with ligand-targeted sterically stabilized nanoparticle. Nucleic Acids Res 2004;32:e149.
[8] Song E, Zhu P, Lee SK, Chowdhury D, Kussman S, Dykxhoorn DM, et al. Antibody mediated in vivo delivery of small interfering RNAs via cell-surface receptors. Nat Biotechnol 2005;23:709–17.

[9] McNamara II JO, Andrechek ER, Wang Y, Viles KD, Rempel RE, Gilboa E, et al. Cell type-specific delivery of siRNAs with aptamer-siRNA chimeras. Nat Biotechnol 2006;24:1005–15.
[10] Li SD, Chen YC, Hackett MJ, Huang L. Tumor-targeted delivery of siRNA by self-assembled nanoparticles. Mol Ther 2008;16:163–9.
[11] Wang XL, Xu R, Wu X, Gillespie D, Jensen R, Lu ZR. Targeted systemic delivery of a therapeutic siRNA with a multifunctional carrier controls tumor proliferation in mice. Mol Pharm 2009;6:738–46.
[12] Davis ME, Zuckerman JE, Choi CHJ, Seligson D, Tolcher A, Alabi CA, et al. Evidence of RNAi in humans from systemically administered siRNA via targeted nanoparticles. Nature 2010;64:1067–70.
[13] Christie RJ, Matsumoto Y, Miyata K, Nomoto T, Fukushima S, Osada K, et al. Targeted polymeric micelles for siRNA treatment of experimental cancer by intravenous injection. ACS Nano 2012;6:5174–89.
[14] Dohmen C, Edinger D, Frohlich T, Schreiner L, Lachelt U, Troiber C, et al. Nanosized multifunctional polyplexes for receptor-mediated siRNA delivery. ACS Nano 2012;26:5198–208.
[15] Lee H, Lytton-Jean AKR, Chen Y, Love KT, Park AI, Karagiannis ED, et al. Molecularly self-assembled nucleic acid nanoparticles for targeted in vivo siRNA delivery. Nat Nanotechnol 2012;7:389–93.
[16] Kim HJ, Ishii T, Zheng M, Watanabe S, Toh K, Matsumoto Y, et al. Multifunctional polyion complex micelle featuring enhanced stability, targetability, and endosome escapability for systemic siRNA delivery to subcutaneous model of lung cancer. Drug Deliv Transl Res 2014;4:50–60.
[17] Jule E, Nagasaki Y, Kataoka K. Surface plasmon resonance study on the interaction between lactose-installed poly(ethylene glycol)-poly(D, L-lactide) block copolymer micelles and lectins immobilized on a gold surface. Langmuir 2002;18:10334–9.
[18] Alam MR, Ming X, Fisher M, Lackey JG, Rajeev KG, Manoharan M, et al. Multivalent cyclic RGD conjugates for targeted delivery of small interfering RNA. Bioconjug Chem 2011;22:1673–81.
[19] Harada A, Kataoka K. Formation of polyion complex micelles in an aqueous milieu from a pair of oppositely-charged block copolymers with poly(ethylene glycol) segments. Macromolecules 1995;28:5294–9.
[20] Kataoka K, Togawa H, Harada A, Yasugi K, Matsumoto T, Katayose S. Spontaneous formation of polyion complex micelles with narrow distribution from antisense oligonucleotide and cationic block copolymer in physiological saline. Macromolecules 1996;29:8556–7.
[21] Kakizawa Y, Kataoka K. Block copolymer micelles for delivery of gene and related compounds. Adv Drug Deliv Rev 2002;54:203–22.
[22] Miyata K, Nishiyama N, Kataoka K. Rational design of smart supramolecular assemblies for gene delivery: chemical challenges in the creation of artificial viruses. Chem Soc Rev 2012;41:2562–74.
[23] Kim HJ, Oba M, Pittella F, Nomoto T, Cabral H, Matsumoto Y, et al. PEG-detachable cationic polyaspartamide derivatives bearing stearoyl moieties for systemic siRNA delivery toward subcutaneous BxPC3 pancreatic tumor. J Drug Target 2012;20:33–42.
[24] Kakizawa Y, Harada A, Kataoka K. Environment-sensitive stabilization of core-shell structured polyion complex micelle by reversible cross-linking of the core through disulfide bond. J Am Chem Soc 1999;121:11247–8.
[25] Matsumoto S, Christie RJ, Nishiyama N, Miyata K, Ishii A, Oba M, et al. Environment-responsive block copolymer micelles with a disulfide cross-linked core for enhanced siRNA delivery. Biomacromolecules 2009;10:119–27.
[26] Christie RJ, Miyata K, Matsumoto Y, Nomoto T, Menasco D, Lai TC, et al. Effect of polymer structure on micelles formed between siRNA and cationic block copolymer comprising thiols and amidines. Biomacromolecules 2011;12:3174–85.
[27] Meister A, Anderson ME. Glutathione. Annu Rev Biochem 1983;52:711–60.
[28] Saito G, Swanson JA, Lee KD. Drug delivery strategy utilizing conjugation via reversible disulfide linkages: role and site of cellular reducing activities. Adv Drug Deliv Rev 2013;55:199–215.
[29] Soutschek J, Akinc A, Bramlage B, Charisse K, Constien R, Donoghue M, et al. Therapeutic silencing of an endogenous gene by systemic administration of modified siRNAs. Nature 2004;432:173–8.
[30] Oba M, Miyata K, Osada K, Christie RJ, Sanjoh M, Li W, et al. Polyplex micelles prepared from ω-cholesteryl PEG-polycation block copolymers for systemic gene delivery. Biomaterials 2011;32:652–63.
[31] Oba M, Fukushima S, Kanayama N, Aoyagi K, Nishiyama N, Koyama H, et al. Cyclic RGD peptide-conjugated polyplex micelles as a targetable gene delivery system directed to cells possessing αvβ3 and αvβ5 integrins. Bioconjug Chem 2007;18:1415–23.
[32] Matsumoto Y, Nomoto T, Cabral H, Mastumoto Y, Watanabe S, Christie RJ, et al. Direct and instantaneous observation of intravenously injected substances using intravital confocal micro-videography. Biomed Opt Express 2010;1:1209–16.
[33] Ruoslahti E. RGD and recognition sequences for integrins. Annu Rev Cell Dev Biol 1996;12:697–715.
[34] Xiong J, Stehle T, Zhang R, Joachimiak A, Frech M, Goodman S, et al. Crystal structure of the extra-cellular segment of integrin αvβ3 in complex with an Arg-Gly-Asp ligand. Science 2002;296:151–5.
[35] Itaka K, Yamauchi K, Harada A, Nakamura K, Kawaguchi H, Kataoka K. Polyion complex micelles from plasmid DNA and poly(ethyleneglycol)-poly(L-lysine) block copolymer as serum-tolerable polyplex system: physicochemical properties of micelles relevant to gene transfection efficiency. Biomaterials 2003;24:4495–506.
[36] Zukerman JE, Choi CHJ, Han H, Davis ME. Polycation-siRNA nanoparticles can disassemble at the kidney glomerular basement membrane. Proc Natl Acad Sci U S A 2012;109:3137–42.
[37] Shayakhmetov DM, Eberly AM, Li ZY, Lieber A. Deletion of penton RGD motifs affects the efficiency of both the internalization and the endosome escape of viral particles containing adenovirus serotype 5 or 35 fiber knobs. J Virol 2005;79:1053–61.
[38] Symonds P, Murray JC, Hunter AC, Debska G, Szewczyk A, Moghimi SM. Low and high molecular weight poly(L-lysine)s/poly(L-lysine)-DNA complexes initiate mitochondrial-mediated apoptosis differently. FEBS Lett 2005;579:6191–8.
[39] Wolfrum C, Shi S, Jayaprakash KN, Jayaraman M, Wang G, Pandey RK, et al. Mechanisms and optimization of *in vivo* delivery of lipophilic siRNAs. Nat Biotechnol 2007;25:1149–57.

Precise Engineering of siRNA Delivery Vehicles to Tumors Using Polyion Complexes and Gold Nanoparticles

Hyun Jin Kim,[†] Hiroyasu Takemoto,[‡] Yu Yi,[§] Meng Zheng,[⊥] Yoshinori Maeda,[§] Hiroyuki Chaya,[⊥] Kotaro Hayashi,[§] Peng Mi,[‡] Frederico Pittella,[⊥] R. James Christie,[⊥] Kazuko Toh,[⊥] Yu Matsumoto,[⊥] Nobuhiro Nishiyama,[‡] Kanjiro Miyata,[⊥,*] and Kazunori Kataoka[†,§,⊥,∥,*]

[†]Department of Materials Engineering, Graduate School of Engineering, The University of Tokyo, Tokyo 113-8656, Japan, [‡]Polymer Chemistry Division, Chemical Resources Laboratory, Tokyo Institute of Technology, Yokohama 226-8503, Japan, [§]Department of Bioengineering, Graduate School of Engineering, The University of Tokyo, Tokyo 113-8656, Japan, [⊥]Center for Disease Biology and Integrative Medicine, Graduate School of Medicine, The University of Tokyo, Tokyo 113-0033, Japan, and [∥]Center for NanoBio Integration, The University of Tokyo, Tokyo 113-8656, Japan

ABSTRACT For systemic delivery of siRNA to solid tumors, a size-regulated and reversibly stabilized nanoarchitecture was constructed by using a 20 kDa siRNA-loaded unimer polyion complex (uPIC) and 20 nm gold nanoparticle (AuNP). The uPIC was selectively prepared by charge-matched polyionic complexation of a poly(ethylene glycol)-*b*-poly(L-lysine) (PEG-PLL) copolymer bearing ~40 positive charges (and thiol group at the ω-end) with a single siRNA bearing 40 negative charges. The thiol group at the ω-end of PEG-PLL further enabled successful conjugation of the uPICs onto the single AuNP through coordinate bonding, generating a nanoarchitecture (uPIC-AuNP) with a size of 38 nm and a narrow size distribution. In contrast, mixing thiolated PEG-PLLs and AuNPs produced a large aggregate in the absence of siRNA, suggesting the essential role of the preformed uPIC in the formation of nanoarchitecture. The smart uPIC-AuNPs were stable in serum-containing media and more resistant against heparin-induced counter polyanion exchange, compared to uPICs alone. On the other hand, the treatment of uPIC-AuNPs with an intracellular concentration of glutathione substantially compromised their stability and triggered the release of siRNA, demonstrating the reversible stability of these nanoarchitectures relative to thiol exchange and negatively charged AuNP surface. The uPIC-AuNPs efficiently delivered siRNA into cultured cancer cells, facilitating significant sequence-specific gene silencing without cytotoxicity. Systemically administered uPIC-AuNPs showed appreciably longer blood circulation time compared to controls, *i.e.*, bare AuNPs and uPICs, indicating that the conjugation of uPICs onto AuNP was crucial for enhancing blood circulation time. Finally, the uPIC-AuNPs efficiently accumulated in a subcutaneously inoculated luciferase-expressing cervical cancer (HeLa-Luc) model and achieved significant luciferase gene silencing in the tumor tissue. These results demonstrate the strong potential of uPIC-AuNP nanoarchitectures for systemic siRNA delivery to solid tumors.

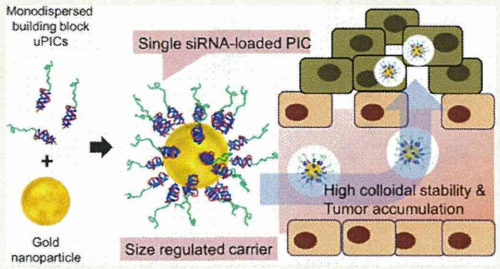

KEYWORDS: siRNA delivery · unimer polyion complex · gold nanoparticle · cancer therapy

Small interfering RNA (siRNA), which induces the sequence-specific degradation of mRNA in the cytoplasm (termed RNA interference (RNAi)), has attracted much attention in cancer therapy.[1,2] However, systemically administered siRNA is rapidly degraded by RNases in the bloodstream and/or eliminated through kidney filtration because they are smaller than 6 nm.[3,4] Thus, siRNA carriers need to be developed in order to overcome these issues for successful therapy. A variety of synthetic nanocarriers have been constructed mainly with cationic nanomaterials, such as lipids, polycations, inorganic nanoparticles, and their hybrid systems.[5−10] These nanocarriers can protect siRNA from enzymatic degradations and apparently increase its size to circumvent kidney filtration. This allows the siRNA payloads to accumulate in tumor tissues through the leaky tumor vasculature *via* the so-called enhanced permeability and retention (EPR) effect.[11,12] In this regard, several recent studies have revealed that precise size-tuning promotes the selective accumulation of nanoparticles in tumor tissues.[13,14] Nanoparticles with a size that is smaller than 50 nm can efficiently

* Address correspondence to kataoka@bmw.t.u-tokyo.ac.jp, miyata@bmw.t.u-tokyo.ac.jp.

Received for review April 17, 2014 and accepted August 18, 2014.

Published online August 18, 2014
10.1021/nn502125h

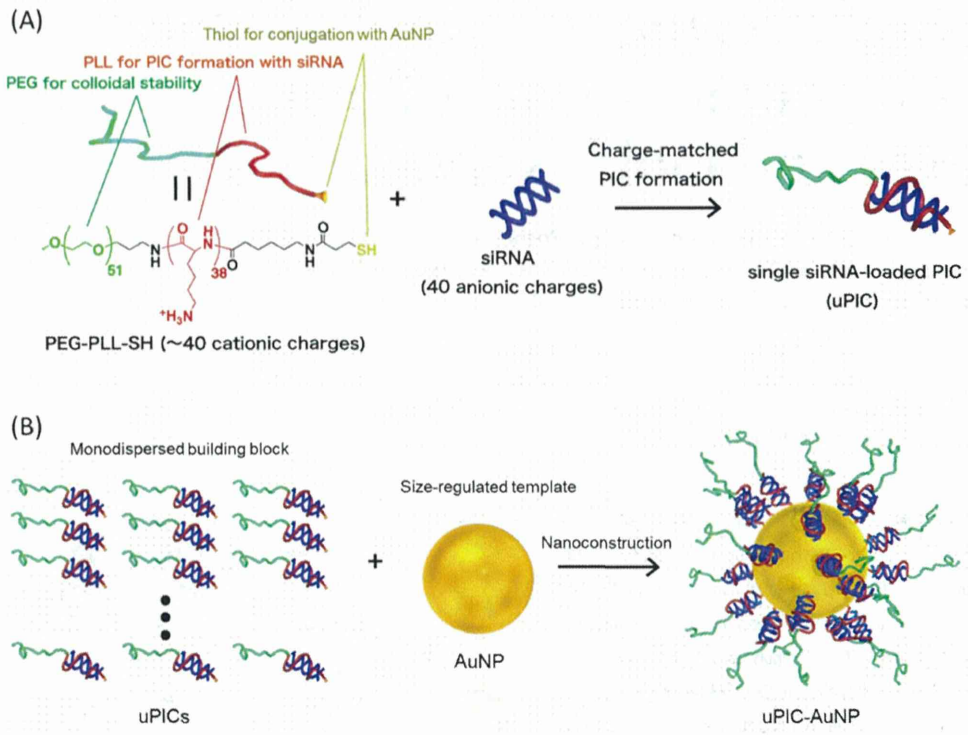

Figure 1. Schematic illustration showing the nanoconstruction of uPIC-AuNPs from monodispersed building blocks. (A) *Formation of uPICs comprising a single pair of PEG-PLL and siRNA.* (B) *Thiol-gold coordination complex between uPICs and AuNP.*

accumulate in tumor tissues, especially in a poorly permeable pancreatic tumor model.[13] Thus, the size of nanocarriers is important for enhancing siRNA accumulation in a variety of tumor tissues.

While multimolecular self-assemblies of siRNA with oppositely charged nanomaterials have been widely developed because of their facile and efficient encapsulation of siRNA, it is difficult to control the size and the distribution of these carriers. In contrast, the bottom-up nanocarrier construction with monodispersed building blocks and a nanotemplate enables more precise size-tuning at the nanoscale. With regard to such building blocks, our recent study demonstrated that a block copolymer of poly(ethylene glycol) and poly(L-lysine) (PEG-PLL) with a controlled degree of polymerization of PLL (DP_{PLL}) formed a unimer polyion complex (uPIC)[15] comprising a single siRNA molecule,[16,17] potentially serving as a monodispersed building block. A building-block-loading nanotemplate is necessary to satisfy the Janus-type property requirement for the selective siRNA release into the cytosol. Gold nanoparticles (AuNPs) are promising biocompatible nanotemplates, as their size can be precisely controlled with a narrow distribution, and also they can be coated with polymers or biomolecules through thiol chemistry.[18,19] This type of bonding is relatively stable under extracellular conditions, but these polymers or biomolecules can be competed off the AuNP with glutathione (GSH), which is abundant in the cytosol.[20] Subsequently, the GSH-coordinated anionic AuNPs may interact with uPICs to destabilize them for triggered siRNA release.

To achieve an efficient systemic siRNA delivery to solid tumors, we developed a size-regulated and reversibly stabilized nanoarchitecture (uPIC-AuNP) by utilizing an AuNP template and a monodispersed uPIC building block prepared with a single siRNA/PEG-PLL pair (Figure 1). To this end, a PEG-PLL was prepared to have a DP_{PLL} of ~40 (matched with the negative charges of 21mer/21mer siRNA) and thiol groups at the ω-end of PLL for coordinate bonding with AuNP. After confirming stable binding between single siRNA molecules and copolymers, the resulting uPICs were conjugated to a 20 nm AuNP to build uPIC-AuNP nanoarchitectures exhibiting sizes less than 50 nm and narrow size distributions under biological conditions. The uPIC-AuNPs achieved efficient siRNA accumulation in a subcutaneous tumor model by systemic administration and successfully induced sequence-specific gene silencing in the tumor tissue.

RESULTS AND DISCUSSION

Preparation and Characterizations of uPICs Comprising a Single PEG-PLL/siRNA Pair. PEG-PLL synthesis was targeted to possess 40 positive charges (or DP_{PLL} = 40), as it can complementarily neutralize the negative charges